Directing self-assembly of nanostructures kinetically: Patterning and the Ehrlich-Schwoebel barrier

Chuan-Fu Lin, Ajmi B. H. Hammouda, Hung-Chih Kan, N. C. Bartelt, and R. J. Phaneuf

Directing Self Assembly of Nanostructures Kinetically: Patterning and the Ehrlich Schwoebel Barrier

Chuan-Fu Lin, Ajmi BH Hammouda, Hung-Chih Kan, N.C. Bartelt and R J Phaneuf

Abstract

We present the results of kinetic Monte Carlo simulations of homoepitaxial growth on a patterned substrate in the presence of an extra barrier to a diffusing adatom crossing of steps from above (Ehrlich-Schwoebel barrier) on topographically patterned surfaces. Our results indicate that over a wide range of Ehrlich-Schwoebel barrier heights, incident atom fluxes and temperatures that multilayer islands or "growth mounds" grow in arrangements which are directed by the topographical pattern. Our simulations indicate that a series of arrangements should form as the temperature is changed due to a competition between the temperature-dependent mound size and the pattern period. We compare these predictions with experimental observation of directed mound assembly on nanopatterned GaAs(001).

A means of fast assembly of extremely large numbers of nanostructures with positional and size control will be required if technology is to keep pace with the ever decreasing size scale of devices called for by such timetables as Moore's Law [1] and the international technology roadmap for semiconductors [2]. Directed self-assembly [3], in which a template influences the otherwise spontaneous arrangement of atoms during processes such as growth [4-18] is an appealing candidate for achieving this. Mechanisms by which templates influence control over how atoms assemble are often based upon either local chemistry [3] or strain [19,20]. Here we demonstrate that a

qualitatively different type of mechanism, in which an extra diffusion barrier to an atom crossing a step [21,22] can lead to self assembly of a variety of ordered arrangements of nanometer-sized "mounds" during epitaxial growth on a patterned substrate.

A familiar example of self-assembly is crystal formation, in which atoms align in periodic arrangements which are dictated by local bonding. In this process kinetics limits the degree to which the lowest-energy, ordered arrangements can form. On the other hand, kinetic barriers have long allowed for the fabrication of structures in which atoms are not in their lowest free energy configurations. A particularly interesting type of diffusion barrier at step edges [21,22] has been shown to lead both to the formation of multilayer islands or "mounds" during crystal growth [23-30] and step bunching or meandering instabilities during sublimation [31] or growth [32], respectively. Our recent work on epitaxial growth of GaAs on patterned GaAs(001) substrates showed evidence that this "Ehrlich-Schwoebel" (ES) barrier might play a role in a transient growth instability we observe [33]. Below we investigate the role of the ES barrier during growth on patterned surfaces using kinetic Monte Carlo simulations.

Methods

Our kinetic Monte Carlo simulations are carried out using a Fortran-based code we developed [34,35]. They use a standard solid-on-solid (SOS) description of the growth of a simple cubic crystal. Our SOS model assigns an integer height $z(\vec{R}_{//})$, measured above the average vicinal plane, to each point $\vec{R}_{//}$ on a square grid of dimensions 500a x 500a, where a is the lattice constant. We use periodic boundary conditions in both directions.

2

The simulations start with a surface containing a square array of flat-bottomed square pits, each of width 50 lattice constants, and with a center to center spacing of 100 lattice constants. We start with pits 10 lattice constants deep, bounded by side walls which form angles of 45 degrees with respect to the surrounding surface.

 The microscopic processes considered are the deposition of atoms with an incident flux F and diffusion; desorption is not considered. In most of the results reported above we fixed the incoming flux at a value corresponding to the arrival of 1 monolayer of atoms per second. Absorbed adatoms hop from site to site in the presence of three energetic barriers: the diffusion barrier, E_d, the in-plane nearest neighbor interaction barrier, E_a and the Ehrlich-Schwoebel barrier, E_{ES}, at step edges. The overall barrier to hopping is

$$E_X = E_d + nE_a + \eta E_{ES} \qquad\qquad (1)$$

Here n is the number of nearest neighbor adatoms with which a diffusing atom interacts; it ranges from 0 to 3, as atoms with 4 neighbors are immobile [34,35]. η is equal to 1 if there is an Ehrlich-Schwoebel barrier for a particular hop, and 0 otherwise. The hopping frequency follows an Arrhenius form with a rate:

$$\Gamma = \nu_0 \exp\left(- E_X / k_B T\right), \qquad\qquad (2)$$

where $\nu_0 = 10^{13}$ Hz is a typical adatom vibration frequency, T is the substrate temperature, and k_B is Boltzman's constant. We use typical values for the diffusion barrier and the in-

3

plane nearest neighbor interaction barrier as 1200 meV and 300 meV , respectively [36], and vary E_{ES}. In the simple model used here no preferential diffusion along step edges is considered.

Results

Example results of our simulations are shown in Fig. 1. In this case the Ehrlich-Schwoebel barrier is set equal to 0.1 eV, a typical for a number of metal surfaces. Fig. 1(a) shows the starting surface, while Figs. 1 (b)-(g) show the topography that results after the simulated growth of a film of 1000 monolayers average thickness at rate of 1 ML/s, and a series of increasing temperatures. Fig. 1 (h) summarizes the average mound size vs. grown thickness for temperatures across this range, and shows that by 1000 monolayers the topography has nearly reached a steady state in each case. Fig. 1(b) is for simulated growth at a temperature of 550K, and shows a high density of irregular mounds decorating the surface. The dendritic shapes of individual mounds indicate that diffusive motion of atoms is slow compared to the arrival of new atoms from the flux at this temperature. Increasing the temperature results in the formation of larger mounds of more regular shapes as can be seen in Figs. 1(c)-1(d). By 680 K a strong correlation between the positions of the mounds and the original pattern is visibly evident. Further increases in the temperature result in even larger mounds, whose shapes evolve from nearly isotropic, to distinctly diamond-like at 725 K, to square at 755K. Growing above this temperature produces mounds whose size exceeds that of the pattern cell, and the shapes become less regular.

4

We statistically analyze the effect of the initial topographical pattern on the self assembly

of the growth mounds, particularly evident in Figs. 1(d), 1(f) and 1(g), using a correlation

function, defined as:

$$G_2(\vec{r}_{//}) \equiv \left\langle \left(z(\vec{R}_{//}) z(\vec{R}_{//} + \vec{r}_{//}) \right) \right\rangle_{\vec{R}_{//}} \qquad (3)$$

In this expression $z(\vec{R}_{//})$ is the local height of the surface at a particular lateral

position $\vec{R}_{//}$, $z(\vec{R}_{//} + \vec{r}_{//})$ is the height at position displaced laterally from this by $\vec{r}_{//}$ and

$\left\langle \ \right\rangle_{\vec{R}_{//}}$ denotes the average over all values of $\vec{R}_{//}$. Maps of this correlation function from

KMC simulations of growth at 550K, 680K 725K and 755K are shown in Figs. 2(a)-(d).

The height of the central peak in each of these maps is equal to the mean-square

corrugation amplitude, with contributions from both the mounds that assemble

spontaneously during growth and what remains of the original pattern. The height of the

"first-order" peaks, i.e. those displaced from the map center by a distance equal to the

pattern period A along the horizontal <100> and vertical <010> directions, gives a

measure of the persistence of the pattern during growth. The most interesting features of

these maps are the intermediate, "satellite" peaks whose positions correspond to

separations between mounds. The observed series of regular arrays of satellite peaks in

the correlation maps confirms the impression obtained from a visual inspection of the

simulated images of Figure 1: that arrangement of mounds locks into a series of ordered

arrays whose period is related to that of the pattern as the temperature is increased. This

behavior is in sharp contrast to what we find for simulated growth on an unpatterned

surface. As seen in Figs. 2(e)-2(h) the corresponding correlation maps for such

simulations show a nearly isotropic ring surrounding an excluded area around the central

5

peak, but otherwise no indication of ordering of the mounds: the arrangement is "liquid-like". The radius of the ring (R_u) in the correlation maps corresponds to the "natural" nearest neighbor mound separation.

An analysis of the positions of the satellites as a function of temperature reveals an intriguing behavior in the assembly of mounds when an initial topographical pattern is present. This can be seen in Fig. 3, where we plot the position of the nearest satellite peaks along both the horizontal <100> and diagonal <110> directions vs. the radius of the ring on the unpatterned surface. The overall behavior seen here is reminiscent of "devil's staircases", or sequences of higher-order commensurate phases which form as temperature or pressure are changed in adsorbate systems when there is a competition between preferred adsorbate-spacings and substrate periodicities [38]. For growth at or below 600K the distances from center of the closest satellites along both of these directions are equal and given by the radius of the ring (R_u). At these low temperatures the mound separations are thus isotropic, and relatively insensitive to the presence of the pattern, which shows up as a background in the correlation maps. By a growth temperature of 660K the pattern clearly exerts an influence on the mound spacing: the symmetry of the satellites visually indicates that the mounds assemble into a square lattice, with the ratio of the distances to the nearest diagonal satellite and to the nearest horizontal satellite in the ratio of √2:1. Interestingly, the mound lattice has adopted a lattice spacing of A/3, rather than the "natural" value of 0.26A which it would have in the absence of the pattern.   It remains locked in to this structure up until a temperature of 700K, in spite of an increase in the unpatterned mound spacing to 0.43A. An analysis of

6

Figs. 1(d), (e) indicates that there is a strong tendency for a single mound to form within each pit, pinning the arrangement of mounds to that of the pattern, with two mounds forming in the bridge between pits. Increasing the growth temperature slightly, to 710K, causes an abrupt change in the arrangement in which the mounds assemble. Evidently driven by the significantly larger natural spacing, the mound lattice rotates by 45 degrees, and adopts an (A/√2x A/√2) unit cell; satellites appear only along <110> directions. The simulated images in this range (e.g. Fig.1(f)) show that a single mound forms in each bridge-site between near-neighbor pits; mounds do not form within pits at these temperatures. As for the lower temperature (A/3 x A/3) structure, the mounds lock into this lower coverage structure over a range of temperature, up to 735K. Raising the temperature to 740K causes the mounds to assemble into a third, even lower coverage arrangement in which all satellites are absent in the correlation maps. The simulations show that the larger natural spacing of the mounds is accommodated by the assembly of individual mounds in the 4-fold sites between pits. At the approximate center of the temperature range for this structure, 755K, the pattern period A coincides with the spacing mounds would naturally adopt. Increasing the growth temperature above 770K results in a disordered structure; there is no simple relation of the placement of these large mounds to the topographical pattern, and even the first-order peaks are absent in the correlation maps.

One might wonder how general the series of self-assembled mound structures seen in Figs. 1 – 3 is. In particular: would a different set of barriers produce mound structures with different periods? To address this we also carried out additional simulations,

varying the diffusion barrier (E_d) from 0.8 eV to 1.2 eV, the in-plane nearest neighbor

interaction barrier (E_a) from 0.25 eV to 0.4 eV, and the Ehrlich-Schwoebel barrier (E_{ES})

from 0.05 eV to 0.2 eV. In each case the same sequence of structures occur, although at

different temperatures ranges. Evidently these directed self assembly structures should

occur over a range of energy barriers on surfaces and incident fluxes.

Our simulations indicate that it should be possible to use patterning to direct the assembly

of nanometer-size mounds into a series of structures in which the spacings are directed by

the pattern. What does this mean about the sizes of the mounds? Interestingly, as shown

in Fig. 4, we find that the mound sizes show some differences from what might be

guessed from the temperature dependence of the correlation map satellite positions. No

obvious break in the dependence of the mound size on temperature is seen in the range in

which the (1/3x1/3) structure forms. Our analysis shows a continuous decrease in the

intensity of the nearest satellite along <100> relative to that along <110> as the

temperature is increased from 670K to 700K, indicating that the mound lattice

accommodates the increase in natural size by a continuous increase in the fraction of near

neighbor mound-pairs which are separated along <110>, rather than <100> directions in

this range. Indeed such a change in the near-neighbor arrangement of mounds is evident

by comparing Figs.1(d) and 1(e).

An interesting question concerns how the choice of initial geometrical parameters might

affect which ordered mound arrangements occur for growth on a patterned surface. To

investigate this we carried out additional simulations for geometries in which the relative

values of different pattern length scales are changed. We find that changing the depth of the pattern at fixed width and pitch has a subtle effect, as summarized in Fig. 5a for the case of the same pattern pitch and pit-width as in Figs. 1-3, but with the depth tripled to h = 30a. The same sequence of phases as in the h = 10a case occurs, with only changes in the transition regions between them. This may be in part due to the finite sidewall angle which causes a decrease in the widths of the flat mesa widths between pits with increasing pit depth.   On the other hand, changing the starting pit-widths for a fixed pitch and depth gives rise to a different sequence of mound structures with increasing temperature. Figure 5(b) summarizes the results for growth simulations in which the pitch and depth are maintained at the same values as in Figs. 1-3, but in which the initial width of the pits is 0.75 times the pitch, i.e. w=75a. In this case the simulations predict four, rather than three ordered mound structures, with unit meshes given by A/5 x A/5, A/3 x A/3, A/2 x A/2 and A x A as the growth temperature is increased. Interestingly, the rotated A/√2 x A/√2 structure is "missing" in this case.

We do not have a detailed understanding of the relationship between the pattern parameters and the mound structures which form, however we expect that it involves a competition between a temperature-dependent natural nearest neighbor mound spacing, discussed above, and the pattern lateral length scales. The mound-pattern interaction is seemingly based upon the formation of mounds only on the flat mesas around, and at the bottoms of pits; this restricts the configurational entropy of mounds on the surface, and results in an effective interaction which is entropic in nature.

9

Are there any real physical systems which show evidence for pattern-directed assembly of growth mounds? The answer is possibly yes. In recent work our group has explored the effect of lithographically patterning GaAs(001) surfaces on the subsequent topography which evolves as more GaAs is deposited, "homoepitaxial growth". In our first experiments we used photolithography followed by etching to create patterns in which the dimensions and spacings of the pits were microns, much larger than the nanometer scale structures we explored in our simulations. Nevertheless, these experiments produced interesting results which suggest that a small Ehrlich-Schwoebel barrier is present on these surfaces, at least for steps of a certain orientation. Specifically, on these "micro-patterned" surfaces we found that depositing Ga and As_2 (the latter in excess) at a temperature of 500ºC and a rate of 1 monolayer per second results in the formation of mounds selectively at the edges of pits along [110] directions [33]. At these length scales, the pits are apparently too far apart to result in formation of ordered mound arrangements between them. More recently we have implemented electron beam lithography to make structures whose dimensions and spacings are much smaller, approaching those used in the simulations.

Fig. 6 shows a series of atomic force microscopy maps of the topography which results from GaAs growth on such nanopatterned (001) surfaces at two different temperatures. At the lower of the two temperatures, 460ºC, individual mounds span bridges between neighboring pairs of nanopits separated along [110] directions, ("[110] two-fold bridges"). It is at these same sites that mounds form in the second ordered arrangement, $A/\sqrt{2}$ x $A/\sqrt{2}$ structure, in the simulations for the first pattern geometry discussed above

10

(Fig. 1(f)). A difference is that the mounds which form at the centers of the two-fold

bridges along [1$\underline{1}$0] directions in the simulations are missing in the experiments. The

GaAs(001) surface, in fact is not 4-fold symmetric: both the Ga diffusivity [37,39] and

adatom-step sticking probabilities [40] are different along [110] and [1$\underline{1}$0], as is the

geometry of steps running along [110] ("B-type") and [1$\underline{1}$0] ("A-type") for both the

c(4x4) [37] of interest here and the β2(2x4) reconstruction [39-44] which occurs above

~550C [33,45]. In addition, our earlier results on micropatterned GaAs(001) suggested

the presence of a finite Ehrlich-Schwoebel barrier along [110] but not obviously along

[1$\underline{1}$0]. The height gray belts on Figure 5 reflect these effects Even more striking is the

observation after increasing the experimental growth temperature to 525°C. In this case

mounds again form at the centers of the "four-fold bridges" between the corners of

nanopit neighbors, and lead to the same AxA structure seen at the higher temperatures in

the simulations (Fig. 1(g)). Additional preliminary experiments at lower temperatures

than those explored here suggest that directed assembly of higher density mound

structures is possible as well [45].

Discussion

We now consider how an artificially imposed topographical pattern might act in directing

the assembly of mounds during growth. One possibility is based upon the modification

of the local density of adatoms on the surface. On relatively flat regions of a surface

such as those between the pits, growth via the formation of atom clusters ("islands") is

favored over the addition of atoms to existing steps. As islands are most likely to form

where adatom density is high, a seeming explanation for our observations is that the

11

positions of the maxima in the adatom density relative to the pattern changes with temperature owing to thermal activation across the Ehrlich-Schwoebel barriers at the edges of pits. This possibility, however, is ruled out by a simple solution of the diffusion equation, which shows that initially the adatom density is always at the 4-fold bridge sites; a moderate Ehrlich-Schwoebel barrier flattens this maximum out, but does not shift its position [46]. Initially this favors island formation near the centers of the bridges between pits. We thus consider a second possibility, suggested by the inset of Fig. 4, that beneath 700K the mound sizes on the patterned surfaces follow those determined by kinetics in the absence of a pattern. This natural size arises from the competition of the Ehrlich-Schwoebel barrier, which favors vertical growth of multi-island stacks [24-31], and arrival of diffusing adatoms on the underlying surface favors lateral growth due to attachment to the edges of the bottom-most island. For this to be the correct explanation the mound positions would need to evolve during growth from the initial nucleation sites favored by highest adatom density to relative positions determined by their natural size, and the effects of the pattern. One of these is the reduction of the area of the underlying terrace, and thus the supply of adatoms for lateral growth, if a mound approaches the upper edge of a pit. Some evidence for this evolution is seen in Figure 7, which shows series of height profiles from our simulations for increasing grown thickness. Successive panels in this figure are for temperatures corresponding to the centers of the ranges in which the three ordered mound structures assemble for the pattern geometry of Fig. 1. For the A/3 x A/3 arrangement of mounds seen in Fig. 1(d) two mounds can be accommodated in the bridge between near-neighbor pits, with a third forming in the pit bottoms; in Figure 7(a) an initial height maximum forms near the center of the 2-fold

12

bridge, as expected based on the adatom density, but two maxima evolve near the bridge edges as the growth continues. Raising the temperature increases the rate of atom diffusion, and thus the natural size of the mounds. Larger mounds are accommodated by the 2-fold bridge sites in the $A/\sqrt{2} \times A/\sqrt{2}$ structure, and the largest in the 4-fold bridge sites of the AxA structure.

The model used in our simulations is extremely simple, and leaves out many effects, including elastic strain near the edges of pits, interaction between steps like those that bound the pits and anisotropy in the diffusivity and atom-step attachment probabilities. Nonetheless the simulations along with early experimental results are suggest that indeed the extra, "Ehrlich-Schwoebel" barrier, which impedes atoms crossing steps from above, and has long known to produce mounds during growth on certain surfaces [24-31] might be exploited to direct the arrangement of such mounds on a patterned surface.

Conclusions

In summary, our results show that a purely kinetic effect, i.e. an additional diffusion barrier at step edges can act not merely to suppress the lowest energy atom arrangement during growth, but to direct a series of ordered arrangements of nanometer-sized mounds with temperature, by controlling the competition between the natural mound near neighbor spacing and the length scales imposed by an artificially produced pattern. The sequence of mound structures varies with the pattern length scales. Most importantly, the density of mounds in these structures can exceed that of the initial pattern. We anticipate

13

that this phenomenon could find application in the fast, controlled assemblies of nanostructures called for by current technology.

14

References

[1] Moore, G.E. Cramming more components onto integrated circuits. Electronics, **38**, 1965, pp. 114–117.

[2] http://www.itrs.net/reports.html

[3] See, for example, S. Mann, Nature Materials **8**, 781 (2009).

[4] T. I. Kamins and R. S. Williams, Appl. Phys. Lett. **71**, 1201 (1997)

[5] A. Konkar, R. Heitz, T. R. Ramachandran, P. Chen, and A. Madhukar, J. Vac. Sci. Technol. B **16**, 1334 (1998)

[6] R. Zhang, R. Tsui, K. Shiralagi, D. Convey, and H. Goronkin, Appl. Phys. Lett. **73**, 505 (1998)

 [7] G. Jin, J. L. Liu, and K. L. Wang, Appl. Phys. Lett. **76**, 3591 (2000)

[8] H. Lee, J.A. Johnson, M.Y. He, J.S. Speck, and P.M. Petroff, Appl. Phys. Lett. **78**, 105 (2001)

[9] T. Kitajima, B. Liu, and S. R. Leone, Appl. Phys. Lett. **80**, 497 (2002)

15

[10] T. Ogino, Y. Homma, Y. Kobayashi, H. Hibino, K. Prabhakaran, K. Sumitomo, H. Omi, S. Suzuki, T. Yamashtia, D. J. Bottomley, F. Ling, A. Kaneko, Surface Sci. **514**, 1 (2002)

[11] "Ge island formation on stripe-patterned Si(001) substrates," Z.Y. Zhong, A. Halilovic, M. Mühlberger, F. Schäffler, and G. Bauer, Appl. Phys. Lett. **82**, 445 (2003)

[12] Z.Y. Zhong, A. Halilovic, M. Mühlberger, F. Schäffler, and G. Bauer, J.Appl. Phys. **93**, 6258 (2003)

[13] Z.Y. Zhong, A. Halilovic, T. Fromherz, F. Schäffler, and G. Bauer, Appl. Phys. Lett. **82**, 4779 (2003)

[14] J. L. Gray, S. Atha, R. Hull, and J. A. Floro, Nano Lett. **4**, 2447 (2004)

[15] B. Yang, F. Liu and M. G. Lagally, Phys. Rev. Lett. **92**, 025502 (2004)

[16] R.V. Kukta, G. Petroff, and D. Kouris, J. Appl. Phys. **97**, 033527 (2005)

 [17] J. L. Gray, R. Hull, and J. A. Floro, J. Appl. Phys., **100**, 084312 (2006)

[18] A. Pascale, I. Berbezier, A. Ronda, and P. C. Kelires, Phys. Rev. B 77, 075311 (2008)

16

[19] A. T. N'Diaye, S. Bleikamp, P.J. Feibelman, and T. Michely, Phys. Rev. Lett. **97**, 215501 (2006)

[20] H. Hu, H.J. Gao and F. Liu, Phys. Rev. Lett. **101**, 216102 (2008)

[21] G. Ehrlich and F.G. Hudda, J. Chem. Phys. **44**, 1039 (1966)

[22] R.L. Schwoebel, and E.J. Shipsey, J. Appl. Phys. **37**, 3682 (1966)

[23] M.D. Johnson, C. Orme, A.W. Hunt, D. Graff, J.L. Sudijono, L.M. Sander, and B.G. Orr, Phys. Rev. Lett. **72** 116 (1994)

[24] P. Politi and J. Villain, Phys. Rev. B **54**, 5114 (1996)

[25] J. Camarero, V. Cross, M.J. Capitán, J. Álvarez, S. Ferrer, M.A. Niño, J.E. Prieto, L. Gómez, J. Ferrón, A.L. Vázquez de Parga, J.M. Gallego, J.J. de Miguel and R. Miranda, Appl. Phys. A **69**, 553 (1999)

[26] S. Schinzer, S. Kohler and G. Reents, Eur. Phys. J. B **15**, 161 (2000)

[27] M. Vladimirova, A. Pimpinelli and A. Videcoq, J. Cryst. Growth **222**, 631 (2000)

17

[28] H.-C. Kan, S. Shah, T. Tadayyon-Eslami, and R. J. Phaneuf, Phys. Rev. Lett. **92**, 146101 (2004)

[29] Z-J. Liu and Y.G. Shen, Surface Sci. **595** 20 (2005)

[30] A.B.H. Hamouda, A. Pimpinelli and R.J. Phaneuf, Surface Sci. **602**, 2819 (2008)

[31] J. Krug, V. Tonchev, S. Stoyanov, and A. Pimpinelli, Phys. Rev. B **71**, 045412 (2005)

[32] G.S. Bales, G. S. and A. Zangwill, Phys. Rev. B, **41**, 5500 (1990)

[33] T. Tadayyon-Eslami, H.-C. Kan, L.C. Calhoun, and R.J. Phaneuf, Phys. Rev. Lett. **97**, 126101 (2006)

[34] A. Ben-Hamouda, N. Absi, P.E.. Hoggan, and A. Pimpinelli, Phys. Rev. B **77** 24530 (2008)

[35] A.B. Hamouda, A. Pimpinelli, and T.L. Einstein, Surface Sci. **602,** 3569 (2008)

[36] These values are close to those based upon first principles calculations for c(4x4)-GaAs(001) by *Roehl, et al.,* ref. [37].

18

[37] J. Roehl, A. Kolagatla, V.K.K. Ganguri, S.V. Khare, S.V. and R.J. Phaneuf, Phys. Rev. B **82**, 165335 (2010)

[38] P. Bak, Rep. Prog. Phys. **45**, 587 (1982)

[39] M. Itoh, Phys. Rev. B **64**, 045301 (2001)

[40] T. Shitara, D.D. Vvedensky, M.R. Wilby, J. Jhang, J.H. Neave and B.A. Joyce, Phys. Rev. B **46**, 6825 (1992)

[41] G.R. Bell, T.S. Jones and B. A. Joyce, Surface Sci. **429**, L492 (1999)

[42] M. Itoh and T. Ohno, Phys. Rev. B **63**, 125301 (2001)

[43] M. Itoh, G. R. Bell, A.R. Avery, B.A. Joyce, and D.D. Vvedensky, Phys. Rev. Lett. **81**, 633 (1998)

[44] T. Shitara, J. Zhang, J.H. Neave and B.A. Joyce, J. Appl. Phys. **71**, 4299 (1992)

[45] C.-F. Lin, H.-C. Kan, S. Kanakaraju, SC.J.K. Richardson, N.C. Bartelt and R.J. Phaneuf, in preparation (2012).

[46] N.C. Bartelt (unpublished)

19

Figure Captions

Fig.1: Simulated topography vs. growth temperature. (a) initial patterned surface; pits are 50a wide, 10a deep and separated by A=100a center-to-center, where a is the lattice constant.   (b)-(g) simulated topographies after 1000ML grown thickness, at 1 ML/s. Energetic barriers are Ed=1.2 eV, Ea=0.3 eV, EES=0.1 eV. Growth temperatures are: (b) 550K; (c) 650K; (d) 680K; (e) 695K; (f) 725K; (g) 755K; (h) summary of average mound size vs. grown thickness at a series of temperatures; dashed line indicates 1000ML.

Fig.2: Correlation maps for growth on patterned and unpatterned surfaces. After 1000ML grown thickness, at 1 ML/s. (a) growth at 550K on patterned surface showing weak ordering; (b) growth on patterned surface at 680K, showing square ordering; double-dot dash lines show a separation of A/3; (c) growth on patterned surface at 725K, showing diagonally-ordered structure; dotted lines show a pacing of √2A/2; (d) growth at 755K on patterned surface showing original pattern period; 2(e)-(h) growth on un-patterned initial surface showing liquid-like ordering: (e) at 550K; (f) at 680K; (g) at 725K; (h) at 755K; R_u indicates the radius of the ring in the correlation maps, corresponding to the near-neighbor mound separation.

Fig.3: Evidence for lock in of mounds to series of ordered structures. Nearest satellite peak position from correlation maps after growth on patterned surface vs. ring radius for unpatterned surface, along [110] (red open circles) and [100] (blue solid squares). After 1000ML grown thickness, at 1 ML/s, with temperature as indicated. Solid blue line has slope 1, corresponding to mound spacing along [100] equal to that on an unpatterned surface. Solid red line has slope √2. Mound lattice vectors relative to pattern are indicated for three ordered structures. Insets from top to bottom show the correlation maps of surface morphologies after growth at 755K, 725K and 680K, respectively.

Fig.4: Average mound size on patterned vs. unpatterned surfaces. After growth of 1000ML at 1 ML/s, with temperatures as indicated. Insets at lower right are correlation maps for 690K and 700K, as indicated.

Fig.5: Effect of pattern parameters on sequence of mound structures with temperature. Nearest satellite peak position from correlation maps after simulated growth on patterned surface vs. ring radius for unpatterned surface, along [110] (red open circles) and [100] (blue solid squares). After 1000ML grown thickness, at 1 ML/s, with temperature as indicated. (a) Satellite positions for initial pattern pitch A =100a and width w = 50a as for Fig. 3, but depth increased to h = 30a. Insets from top to bottom show the correlation maps of surface morphologies after growth at 740K, 710K and 680K, respectively. (b) Satellite positions for initial pattern pitch A = 100a, depth h = 10a and pit width w = 75a. Insets from top to bottom show the correlation maps of surface morphologies after growth at 760K, 720K, 675K and 630K, respectively.

Fig. 6: Mound structures during growth of GaAs on nanopatterned surfaces. (a) Atomic force microscope image of topography of patterned GaAs(001) before growth.

Pits are 30 nm deep, 150 nm wide and spaced at A = 300 nm. (b) AFM image after growth of 60 nm of additional GaAs at 460ºC. The blue square shows the unit cell of the initial square pattern. (c) After growth of 100 nm at 460ºC. (d) After growth of 30 nm, at a temperature of 525ºC. (e) After growth of 60 nm at 525ºC.

Fig.7: Height profiles of simulated surfaces for increasing amounts of growth. (a)-(b) show the evolution of morphologies of the 2-fold bridges at growth temperatures 680K and 725K, the arrow in (a) indicates a local height maximum near the center of 2-fold bridges at initial stage of growth; (c) shows the evolution of morphologies of the 4-fold bridges. The heights of profiles are rescaled to display subtle features at the early growth stage.
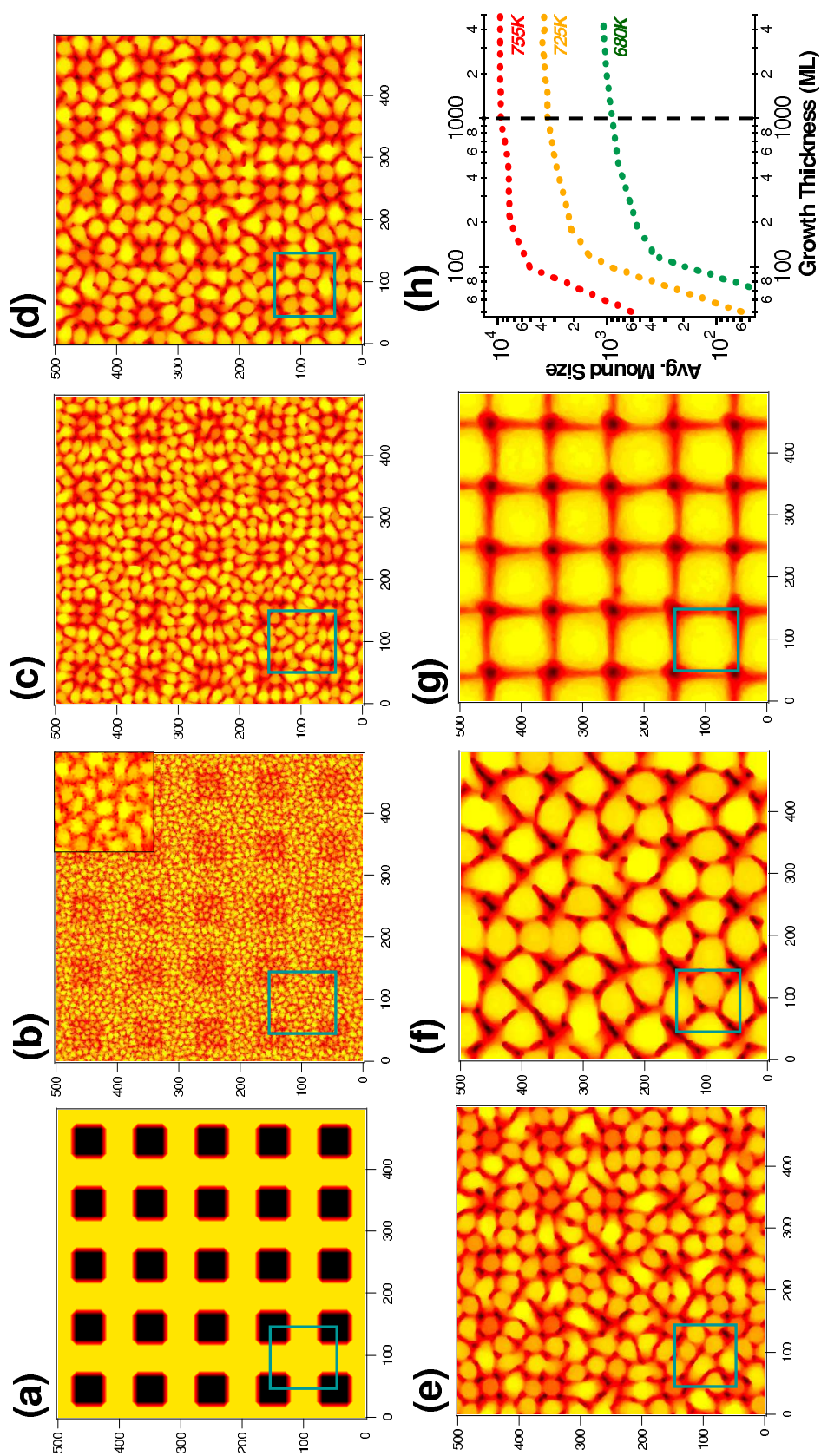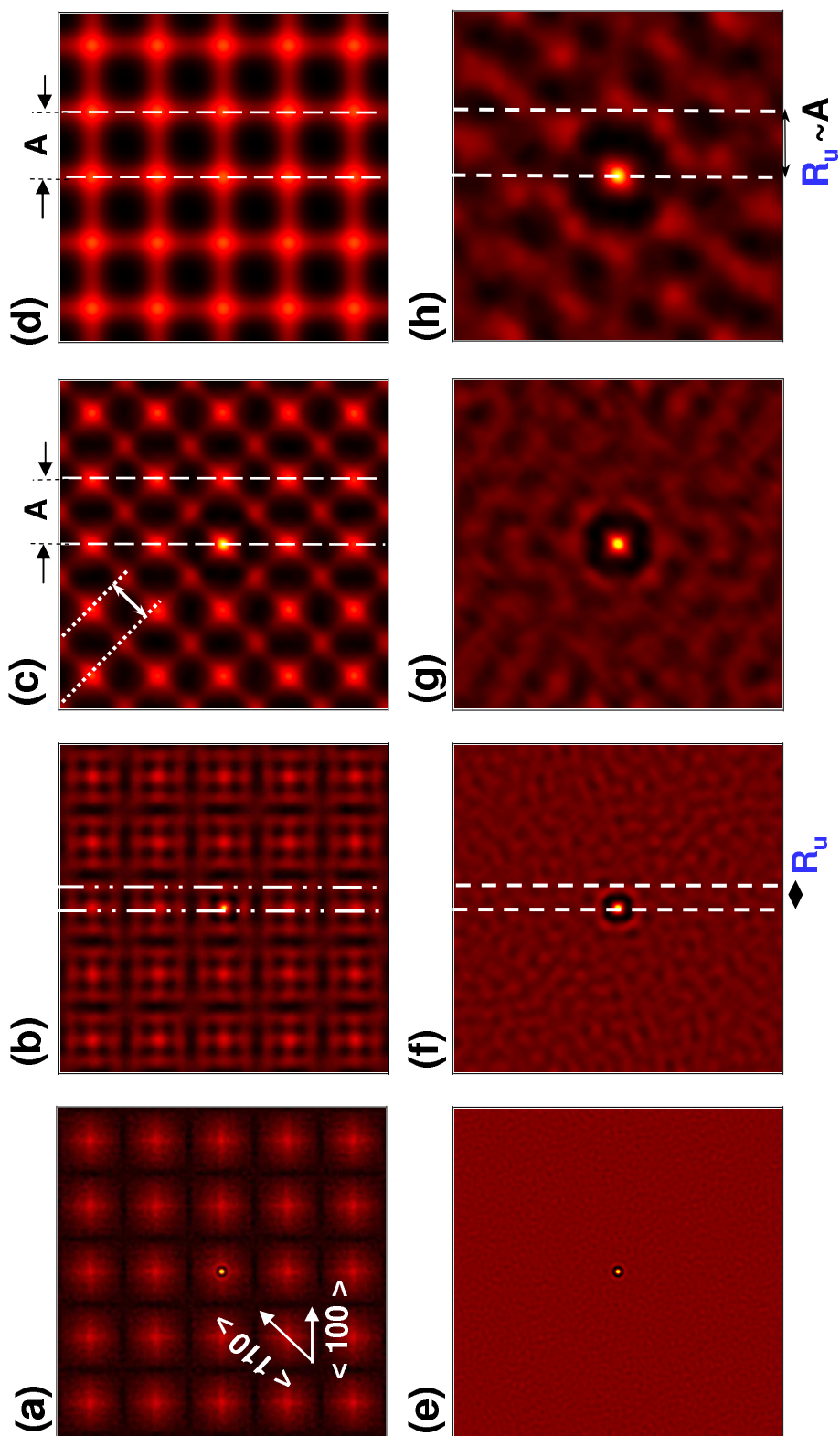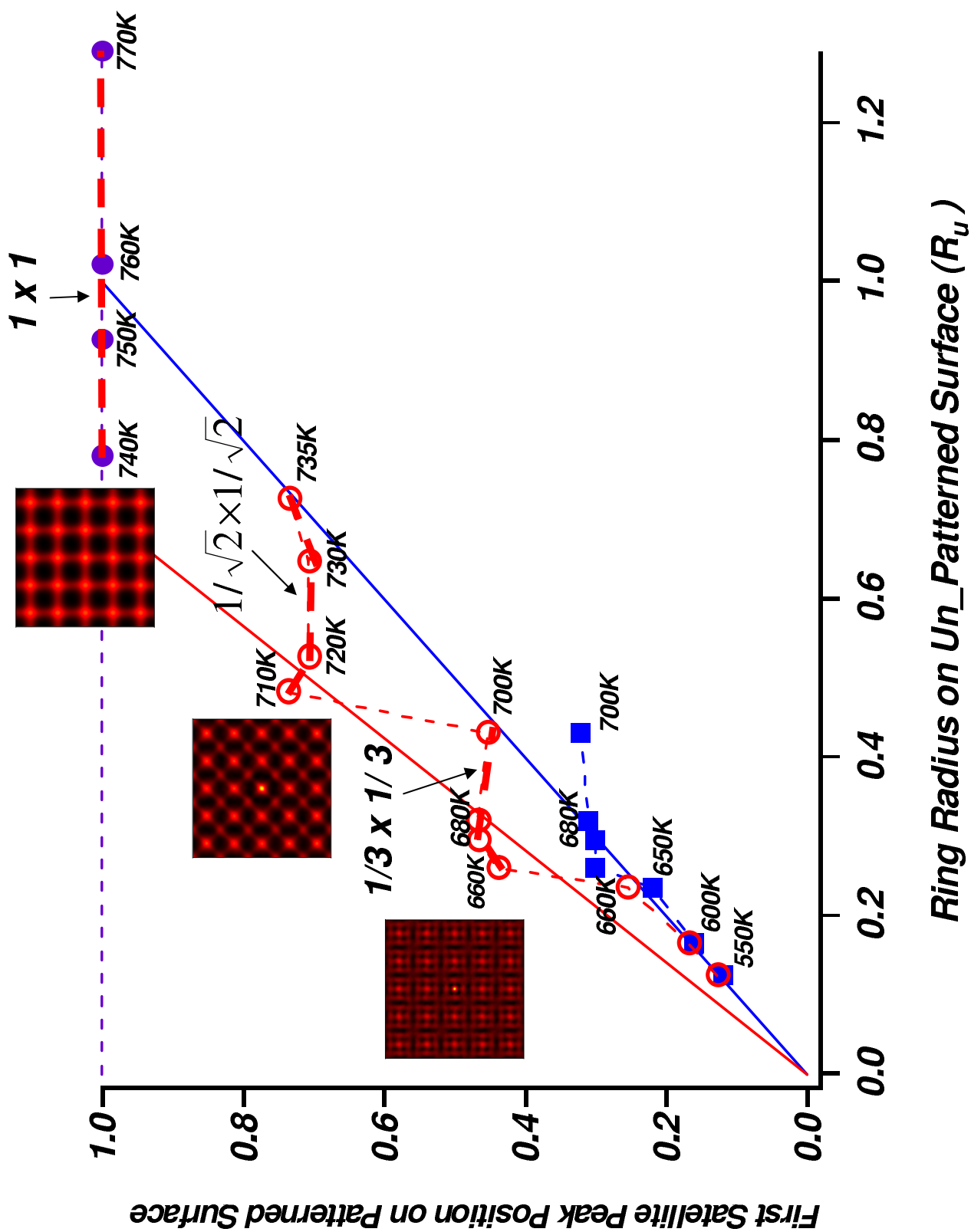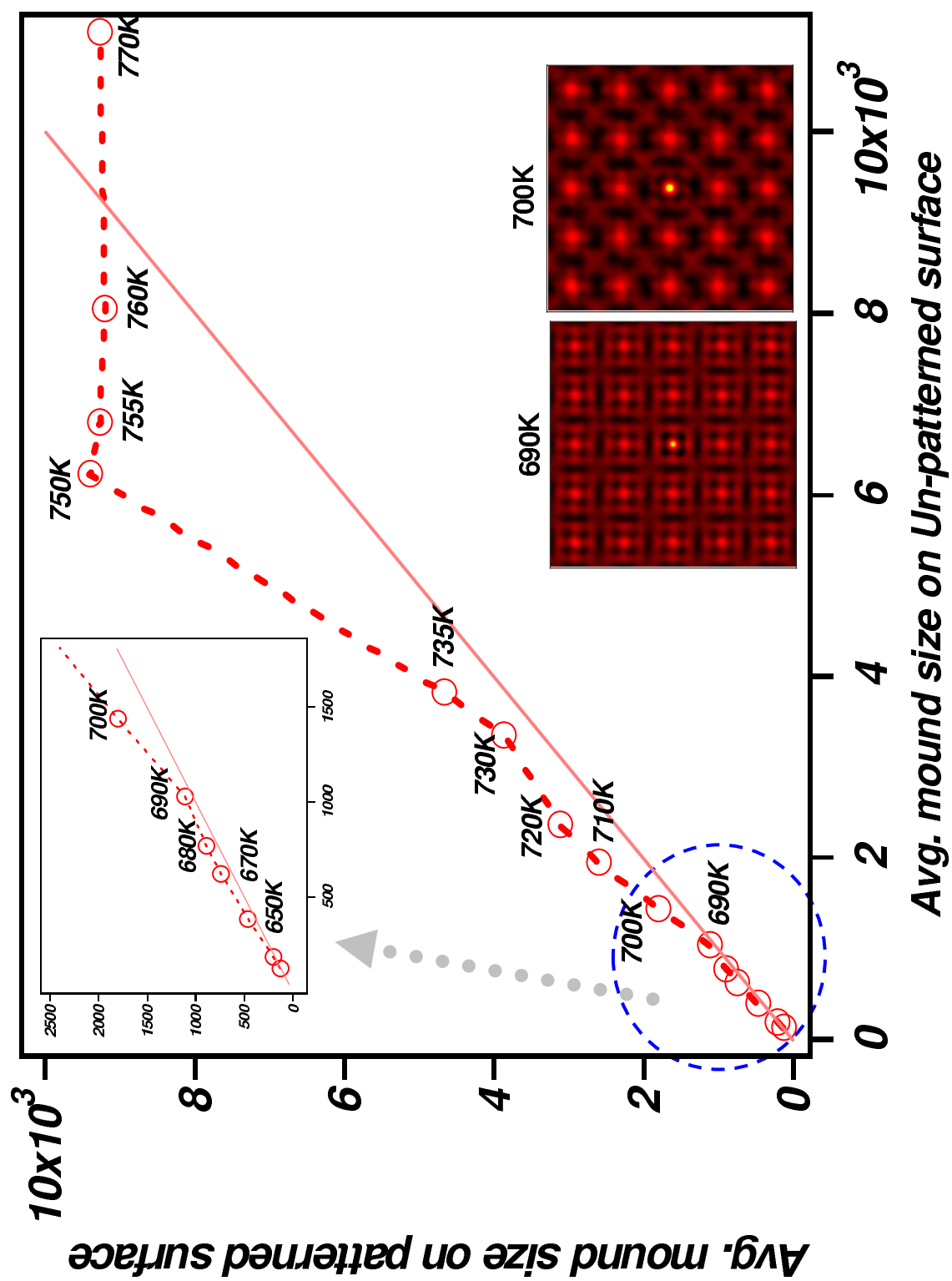
Figure 1   BK11544   19JAN2012

Fig. 2

Figure 2   BK11544   19JAN2012

Fig. 3

Figure 3   BK11544   19JAN2012

Fig. 4

Figure 4   BK11544   19JAN2012

First Satellite Peak Position on Patterned Surface

Ring Radius on Un-Patterned Surface (Ru)

1 x 1

$1/\sqrt{2} \times 1/\sqrt{2}$

760K
750K
740K
730K
725K
710K
695K
690K
670K
650K
625K
600K
550K

Fig.5(a)

Fig.5(b)

Figure 5b   BK11544   19JAN2012

(a) (b) (c) (d) (e)

300nm

[1$\bar{1}$0]

[110]

Fig. 6

Figure 6   BK11544   19JAN2012

Fig. 7

Figure 7   BK11544   19JAN2012